Energy analysis of two-phase secondary refrigeration in steady-state operation, part 2: Exergy analysis and effects of phase change kinetics

Michel Pons, Anthony Delahaye, Laurence Fournaison, Didier Dalmazzone

Accepted Manuscript

Energy analysis of two-phase secondary refrigeration in steady-state operation, part 2: Exergy analysis and effects of phase change kinetics

Michel Pons, Anthony Delahaye, Laurence Fournaison, Didier Dalmazzone
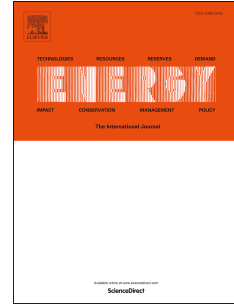
Please cite this article as: Pons M, Delahaye A, Fournaison L, Dalmazzone D, Energy analysis of two-phase secondary refrigeration in steady-state operation, part 2: Exergy analysis and effects of phase change kinetics, *Energy* (2018), doi: 10.1016/j.energy.2018.07.044.

Energy analysis of two-phase secondary refrigeration in steady-state operation,

Part 2: exergy analysis and effects of phase change kinetics

Michel Pons[1][*], Anthony Delahaye[2], Laurence Fournaison[2], and Didier Dalmazzone[3]

1 LIMSI, CNRS, Université Paris-Saclay, Rue J. von Neumann bât 508, 91403 Orsay Cedex, France

2 Irstea, GPAN ENERFRI, 1 Rue Pierre-Gilles de Gennes, CS 10030, 92261 Antony Cedex, France

3 ENSTA ParisTech, Université Paris-Saclay, 828 boulevard des Maréchaux, 91120 Palaiseau, France

* Corresponding author: Michel.pons@limsi.fr

Abstract

A great deal of attention is paid to secondary refrigeration as a means of reducing excessively high emissions of refrigerants (most of which have a potent greenhouse effect) due to leaks in large cooling units. Among the environmentally friendly fluids that can be used in secondary circuits for transporting and storing cold, hydrate slurries offer the advantage of significant latent heats of fusion associated with good fluidity. Research programs have focused attention on hydrate systems, including CO_2, TBPB (tetra-n-butyl-phosphonium-bromide), and mixed CO_2-TBPB hydrates. In addition to feasibility concerns, energy efficiency is also a crucial concern requiring an objective analysis of the improvements likely to result from these new materials. A numerical model of secondary refrigeration system was built for slurries ranging from ice-slurry to TBPB-CO2 mixed hydrate slurries. The circuit was designed for

maximizing performance under various constraints relating to power rate, heat transfer areas, and flow ability. The effects of phase change kinetics on thermal exchanges were introduced in the model and in the exergy balance. The results, analyzed in terms of exergy losses, demonstrate the couplings through which kinetics influences global performance.

Keywords

Refrigeration, second law, phase change material, hydrate, clathrate, slurry, CO2, TBPB, ice.

Nomenclature

Usual notations (T for temperature, P for pressure, $\dot{Q}$ for heat flux, etc.) are not recalled here.

A heat-transfer area [m^2]

B exergy [J]

COP coefficient Of Performance of the primary cooling unit

D diameter (hydraulic) [m]

L distance between the primary cooling unit and the end-user [m]

u flow velocity [m.s^{-1}]

U global heat transfer coefficient [W.m^{-2}.K^{-1}]

x additive concentration in the liquid phase [kg.kg^{-1}]

X solid fraction in the slurry [kg.kg^{-1}]

Y component fraction in the solid phase [kg.kg^{-1}]

Greek symbols

χ mass fraction in the total flow [-]

ϕ solid volume fraction in the slurry [-]

η efficiency (isentropic) [-]

ϕ volume fraction of solid in the slurry

Indexes

0 initial liquid solution *water + additive*

1-7 points in Fig. 1

A additive

C condenser

CD carbon dioxide (CO_2)

cr crystallization

dis by thermal dissipation

E evaporator

eq equilibrium

f fusion

G gas phase

$HX\_$ referred to the corresponding heat exchanger, *C, E* or *U*.

I insulation

in inlet of a HX section

kin by phase change kinetics

L liquid phase

O outdoor air

P slurry pump

PC primary compressor

PCU primary cooling unit

S solid phase (crystals)

T total

U user

vis by viscous friction

W water (H_2O)

3

1 Introduction

One of the challenges facing the refrigeration industry is the need for drastic reduction of its contribution to global warming. Large cooling units are often affected by extensive leaks, while current refrigerants have a Global Warming Potential (GWP) on the order of several thousand [1, 2]. As a result, this industry as a whole contributes up to 8% of total greenhouse-gas emissions. Research on new refrigerants with low GWP is underway, but one solution already exists. It consists of splitting large cooling units into two parts. The first part is the *primary* cooling unit itself, whose volume is reduced as much as possible in order to limit leakage, and which can thus be contained within a technical room. The second part is a *secondary* circuit designed for transporting and distributing cold, and in which the refrigerant is replaced by an environmentally friendly fluid. Among all potential secondary fluids, a new class has become the focus of interest: hydrate slurries. Clathrates hydrates are ice-like crystals in which H_2O molecules form cages around host molecules. These host molecules can be a gas (CH_4, CO_2, etc.), or a quaternary salt such as tetra-n-butyl-ammonium-bromide (TBAB), tetra-n-butyl-phosphonium-bromide (TBPB), or others. *Mixed* hydrates may also form, e.g. CO_2-TBPB hydrates [3-5]. These solid-liquid *slurries* offer several advantages, including the transport of latent heat or fluidity. Moreover, thanks to their wide variety, the phase-change temperature can easily be adapted to the design application. Readers are referred to the bibliography given in Part 1 of this study [9]. As hydrate slurries are attractive options for the purposes of secondary refrigeration and cold storage, they have been studied extensively, particularly with respect to their rheology, thermal properties, and phase-change kinetics [6-8]. Analysis of the energy performance of secondary refrigeration systems is the general objective of this study. A robust analysis framework was constructed and used for comparing and analyzing performance obtained with a selection of slurries [9]. This framework (described in Section 2) was supplemented with the exergy analysis of the system

as a whole (section 3) followed by the introduction of phase-change kinetics (section 4), with unexpected consequences on performance (Section 5).

2   Thermodynamic framework and process optimization

The thermodynamic system considered herein is the global process – the primary cooling unit plus secondary loop – described in Fig. 1. When circulating in the secondary loop 123451 by means of pump *P*, the slurry transports the heat extracted from the *user's* heat exchanger *HXU* to the primary cooling unit, i.e. its evaporator *HXE*, which is located at a distance *L*. The primary compressor *PC* consumes mechanical power, while the condenser *HXC* releases heat outdoors.
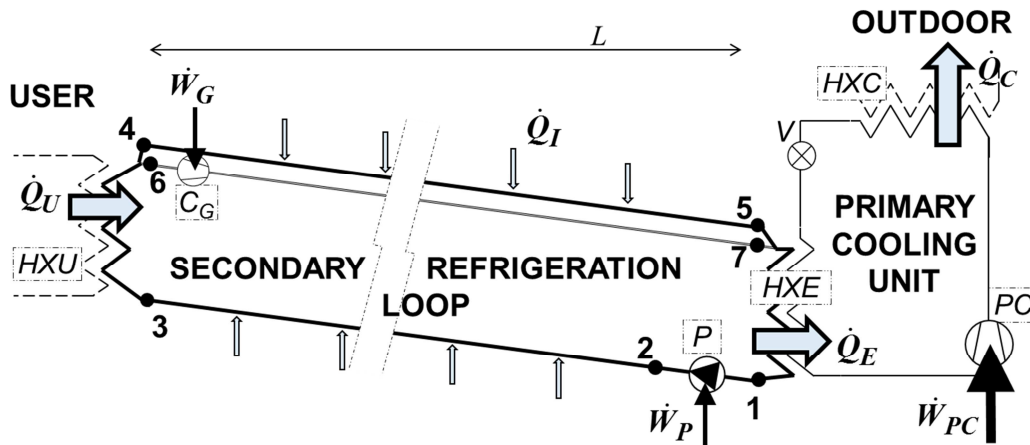
Fig. 1: Schematic of a secondary refrigeration process.
123451: slurry loop; *P*: slurry circulation-pump; *HXU*, *HXE* and *HXC*: heat exchangers on the user's side, at the evaporator and condenser of the primary cooling unit; *PC*: primary compressor; *V*: throttling valve; 67: return line for gaseous CO_2 and C_G: gas compressor (when involved). *L*= distance between user and primary cooling unit.

Four slurries are considered in this study: two of them include carbon dioxide in the hydrate crystals and release gaseous CO_2 upon melting. This vapor is separated from the slurry flow at the outlet of the *HXU* heat exchanger and returns to the crystal generation process in the *HXE* heat exchanger via a specific pipe 67 and a minimum of recompression *CG* compensating for the various pressure drops. The mechanical energy of the two pumps *P* and

CG dissipates into heat, which adds to the flux $\dot{Q}_I$ entering the secondary circuit through its thermal insulation. Equation (1) gives the First Law balance of the system as a whole:

$$\dot{Q}_C = \dot{Q}_U + \dot{Q}_I + \dot{W}_P + \dot{W}_G + \dot{W}_{PC} = \dot{Q}_E \cdot (1 + COP^{-1}) \tag{1}$$

where the Coefficient of Performance of the cooling unit ($COP = \dot{Q}_E / \dot{W}_{PC}$) is given by $COP = T_E \cdot \eta_{PCU} / (T_C - T_E)$.

For the sake of fair comparison, the configuration for each case under consideration (one case = one slurry + one kinetics time constant) is designed according to an optimization approach where the total electrical consumption $\dot{W}_T = \dot{W}_{PC} + \dot{W}_P + \dot{W}_G$ is minimized under the following prescribed constraints, whose meanings are discussed in engineering terms in [9]:

1. The heat flux $\dot{Q}_U$ extracted from the user (i.e. the duty of the process) is prescribed (30kW).

2. The area of the heat exchanger HXE between refrigerant evaporation and crystal generation in the slurry is prescribed (6m^2).

3. The total area of the two heat exchangers $HXU + HXC$ is given (35m^2).

4. The Reynolds numbers lies above 4000 everywhere in the loop tubes and in the HXE, and above 2500 in the HXU heat exchanger.

In addition, the transport distance L equals 50m, the indoor and outdoor air temperatures are T_U=25°C and T_O=40°C, respectively, and the internal Second Law efficiency of the primary cycle η_{PCU} is 0.75.

The four slurries considered herein range from the well-known ice slurry (code IG) to the prospective slurry of mixed hydrate with CO_2+TBPB (code MH). Their thermo-physical characteristics vary widely in terms of enthalpy of fusion, melting temperature, apparent viscosity, and involvement or non-involvement of CO_2 (see Table 1).

6

Code	Description	T_f (°C)	ΔH_f (kJ.kg^{-1})	$\mu_{\phi=0.1}$ (mPa.s)	$\mu_{\phi=0.2}$ (mPa.s)
IG	Ice crystals in solution of monopropylene-glycol (x_0=0.08)	-2.7	333.6	3.5	4.5
CO	CO_2 hydrate in water (P_G=3.03MPa)	7.2	374.0	4	9
TB	TBPB hydrate in solution of TBPB (x_0=0.20)	7.3	204.0	7	17
MH	TBPB+CO_2 mixed hydrate in solution of TBPB (x_0=0.20; P_G=0.72MPa)	12.1	223.6	7	17

Table 1: Description of the four considered slurries, fusion temperature T_f, enthalpy of fusion ΔH_f (per unit mass of melted crystal), and effective dynamic viscosities with ϕ=0.1 and ϕ=0.2 (slurry velocity=1m.s^{-1}; tube diameter=30mm).

3   Exergy and performance analyses

3.1   Exergy analysis

Like in any thermal process, kinetic energy is negligible compared to the enthalpy changes under consideration. Moreover, the phenomena considered herein are heat transfers, pumping, and compression cooling cycle. Exergy is thus defined by its differential $db=dh-T_O \cdot ds$, where *h* and *s* are the enthalpy and entropy of the two- or three-phase *flow* (including the gas phase when present). As there is no mechanical effect in the heat exchangers, one may write: $ds=dh/T$, where *T* is the local *flow* temperature. Deriving literal expressions of exergy fluxes and losses is greatly simplified when using the notion of *entropic mean temperature* defined as follows: when a system undergoes a transformation with the enthalpy and entropy changes Δh and Δs, its entropic mean temperature during that transformation is $T = \Delta h / \Delta s$ [10]. The change of exergy is then simply written as $\Delta b=\Delta h \cdot (1-T_O / T)$. When temperature is uniform, i.e. for the heat sources at T_O or T_U and for the primary refrigerant at T_E or T_C, the entropic mean temperature simply equals $T_\bullet$, with $\bullet$=*O*, *U*, *E*, or *C*. The flow temperature, however, is not uniform along the heat exchangers *HXU* and *HXE*. Two entropic mean

7

temperatures then arise: T_{34} for HXU and T_{51} for HXE. The three equations below describe the exergy losses in the three heat exchangers.

$$\Delta\dot{B}_{HXU} = \dot{Q}_U \cdot \left(T_O / T_{34} - T_O / T_U\right) \tag{2}$$

$$\Delta\dot{B}_{HXE} = (\dot{Q}_U + \dot{Q}_I + \dot{W}_P + \dot{W}_G) \cdot \left(T_O / T_E - T_O / T_{51}\right) \tag{3}$$

$$\Delta\dot{B}_{HXC} = (\dot{Q}_U + \dot{Q}_I + \dot{W}_P + \dot{W}_G + \dot{W}_{PC}) \cdot \left(1 - T_O / T_C\right) \tag{4}$$

Using the same concepts and the usual entropy balance in cooling cycles, the *internal* exergy loss in the Primary Cooling Unit can be written easily as:

$$\Delta\dot{B}_{PCU} = \dot{W}_{PC} \cdot T_O / T_C + (\dot{Q}_U + \dot{Q}_I + \dot{W}_P + \dot{W}_G) \cdot \left(T_O / T_C - T_O / T_E\right) \tag{5}$$

Considering that the heat fluxes related to viscous friction (dissipation of $\dot{W}_P + \dot{W}_G$) and to imperfect thermal insulation of the secondary circuit ($\dot{Q}_I$) are smaller than the heat extraction $\dot{Q}_U$ by two orders of magnitude, the corresponding exergy losses may be written with the simplifying approximation that the corresponding heat rates would be generated in *HXE*:

$$\Delta\dot{B}_{vis} = (\dot{W}_P + \dot{W}_G) \cdot T_O / T_{51} \tag{6}$$

$$\Delta\dot{B}_{dis} = \dot{Q}_I \cdot \left(T_O / T_{51} - 1\right) \tag{7}$$

It will be shown below that $\Delta\dot{B}_{vis}$ and $\Delta\dot{B}_{dis}$ are by far the smallest in the entire budget and play no real role in the analysis. Summing up these six equations leads to the following balance:

$$\dot{W}_{PC} + \dot{W}_P + \dot{W}_G = -\dot{Q}_U \cdot (1 - T_O / T_U) + \sum_{\bullet} \Delta\dot{B}_{\bullet} + \dot{Q}_U \cdot \left(T_O / T_{51} - T_O / T_{34}\right) \tag{8}$$

The left-hand side is the total exergy supplied to the system. The first term on the right-hand side is the exergy delivered by the process to the user. The second term sums up the six

8

exergy losses listed above. The last term can be interpreted when considering the slurry temperature during phase change. When phase change occurs with infinitely fast kinetics, the slurry temperature precisely follows the equilibrium temperature described by the equation of state $T = T_{eq}(x, P_G)$. Combining this equation of state with 1) the relation between the additive fraction x in the liquid phase and the solid fraction χ_S in the flow, resulting from mass conservation, and 2) uniformity of pressure in the heat exchangers, leads to a unique correlation $T_{eq}(\chi_S)$, irrespective of the direction of phase change. The system then exactly follows reverse paths during crystallization and fusion, so that the two entropic mean temperatures T_{34} and T_{51} are equal: when kinetics is infinitely fast, the last term of eq. (8) vanishes. When phase change proceeds at a finite rate, a non-zero driving force takes place between the actual conditions (T, P, χ) and those corresponding to equilibrium. Among other possibilities, this driving force may be stated as a temperature difference ($T - T_{eq}$). As this difference takes opposite signs during crystallization ($T < T_{eq}$) and during fusion ($T > T_{eq}$), the two temperatures T_{34} and T_{51} are indubitably different, with $T_{51} < T_{34}$. When also considering that these two entropic mean temperatures account for all the phenomena involved in the enthalpy and entropy changes, it is concluded that the last term of eq. (8) is the exergy loss due to phase change kinetics:

$$\Delta \dot{B}_{kin} = \dot{Q}_U \cdot \left(T_O / T_{51} - T_O / T_{34} \right) \tag{9}$$

Using $\dot{Q}_U$ as the reference heat flux, non-dimensional energy fluxes and exergy losses can be introduced. They are denoted with lowercase letters instead of uppercase ones according to $w_\bullet = \dot{W}_\bullet / \dot{Q}_U$ and $\Delta b_\bullet = \Delta \dot{B}_\bullet / \dot{Q}_U$. The non-dimensional exergy balance is written as:

$$w_{PC} + w_P + w_G = \left(T_O / T_U - 1 \right) + \sum_\bullet \Delta b_\bullet \;, \tag{10}$$

9

with $\bullet \in \{dis, HXC, HXE, HXU, kin, PCU, vis\}$. The various terms of eq. (10) are interpreted in the exact same way as those in eq. (8).

3.2 Analysis of performance with infinitely fast kinetics

Figure 2 shows the four non-dimensional exergy budgets, one per slurry, calculated with the assumption of infinitely fast kinetics. The total exergy supplied to the process (symbol ►) consists of the delivered exergy ($= T_O / T_U - 1 = 0.0503$, symbol ○) plus the six exergy losses in play. It reproduces the values of total energy consumption w_T presented in Table 1 of ref. [9]: the exergy budget is thus correct. The best performance is obtained with the slurry *MH*, which requires the smallest compression work w_{PC} (0.20 compared to 0.27 for *IG*).
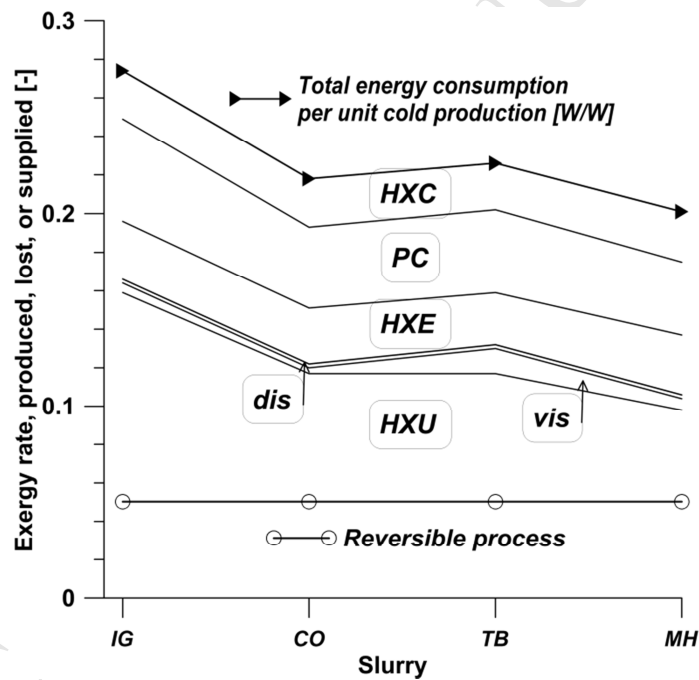
Fig. 2: Non-dimensional performance and exergy analysis for each slurry under consideration (*IG*=Ice+MPG, *CO*=CO$_2$ hydrate, *TB*=TBPB hydrate, *MH*=Mixed TBPB+CO$_2$ hydrate) in thermodynamic equilibrium. The delivered exergy $(T_O / T_U - 1)$ (symbol ○) plus all the exergy losses (in the user's heat exchanger *HXU*, by viscous friction *vis*, by dissipation through thermal insulation *dis*, in the evaporator *HXE*, in the primary cooling unit *PC*, and in the condenser *HXC*, respectively) equals the total exergy input (symbol ⊖).

10

Beyond this raw result, it can also be noticed that the curve w_T (⌒⦙) very closely follows the changes of the fusion temperature T_f reported in Table 1, and not those of ΔH_f nor of viscosity. It is moreover well-known that the COP of the primary cooling cycle is highly dependent on the temperature difference $T_C - T_E$. As the evaporation temperature T_E from *IG* to *MH* (-2.7≤T_E≤+12°C) changes in parallel to T_f (-9.5≤T_f≤+4.4°C), the slurry *MH* finally consumes less mechanical work than the other three ones for the same duty. The exergy analysis also gives another insight. Figure 2 shows that, among the six exergy losses, the one that is reduced when changing slurry from *IG* to *MH* is not Δb_{PCU} in the primary cooling unit, but Δb_{HXU} in the *user's* heat exchanger. Increasing the temperature of fusion T_f reduces the difference $T_U - T_f$ (from 22 for *IG* to 13K for *MH*): the heat transfer area A_{HXU} must be extended accordingly (from 5 to 9 m^2) in order to keep the heat rate $\dot{Q}_U$ unchanged (constraint #1). Increasing heat transfer areas is precisely one means of reducing exergy losses due to heat transfer, and thus of improving the performance of thermal process.

The fact that the exergy loss in the condenser *HXC* is not significantly modified from slurry *IG* to *MH* is the result of two opposite trends. On one hand, the improved COP reduces the heat rate transferred by the condenser $\dot{Q}_{HXC}$. On the other hand, the reduction in heat transfer area A_{HXC} (due to the larger A_{HXU} under constraint #3) tends to raise the temperature T_C. In the present case, these two trends practically cancel out each other.

The exergy budget also shows that Δb_{vis} and Δb_{dis} are negligible. The general design of the process succeeds in keeping both pumping power and heat flux through the insulation at auxiliary levels. This also retroactively justifies the simplification mentioned above concerning these two exergy losses. Finally, it can be seen that the last three exergy losses

Δb_{HXU}, Δb_{PC}, and Δb_{HXC} have similar weights in the budget, as would be expected in a consistently designed unit.

4 Modelling heat transfer with phase change kinetics

The equations describing heat exchanges in a two- or three-phase flow, as presented in Part 1 of this study, must be reconsidered in presence of phase change kinetics because the systems departs from equilibrium. This fundamentally changes the relation between temperature T and solid mass fraction χ_S, the two quantities involved in the enthalpy differential $dh = \overline{c_p} \cdot dT - \Delta H_f \cdot d\chi_S$. (Considering that the pressure drops along the heat exchangers are limited and that they only affect the enthalpy of the gas phase, the mass fraction of which in the *flow* is also limited, it is approximated that the pressure contribution to the enthalpy differential is negligible). In steady-state and 1D geometry, the transport equation for enthalpy in the heat exchangers is then written as:

$$\dot{m} \cdot \left(\overline{c_p} \cdot \frac{dT}{dy} - \Delta H_f \cdot \frac{d\chi_S}{dy} \right) = (U_\bullet \Pi_\bullet) \cdot (T_\bullet - T) \tag{11}$$

where $U_\bullet$ is the global heat transfer coefficient [in W.m^{-2}.K^{-1}] between either the primary refrigerant ($\bullet = E$) or the air-conditioned room ($\bullet = U$), and the secondary *flow* in the heat exchanger, and where $\Pi_\bullet$ is the corresponding heat transfer area per unit length along the heat exchanger ($\Pi_\bullet = dA_{HX\bullet} / dy$).

4.1 A general law for kinetics

Active research is currently underway on phase change kinetics in hydrate slurries [11-14] as well as in ice slurries. Kinetics is a two-fold issue. First, induction, i.e. the time delay before the very first crystals forms in a subcooled solution. This rather unpredictable phenomenon is best avoided in secondary refrigeration systems, e.g. by preventing the solid phase from

melting completely so that the remaining crystals serve as nucleation seeds for the next crystallization. Induction is thus not a concern in this article where the minimal value for the crystal mass fraction X is set to 0.03. Herein, *kinetics* thus means the *rate of phase change* once initiated. Phase change proceeds in the solid-liquid system out-of-equilibrium at a rate that is related to the distance between the actual state and equilibrium. Equilibrium is described by the general equation of state $T_{eq}(x, P_G)$, where the system temperature depends on the mass fraction x of additive in its aqueous solution (when relevant), and on the CO_2 pressure P_G (when present). During phase change, the system temperature T departs from T_{eq}, with $T<T_{eq}$ during crystallization and $T>T_{eq}$ during crystal fusion. Similarly, it can be said that, for a given temperature T, the actual composition x differs from its equilibrium value x_{eq} defined by $T_{eq}(x_{eq}, P_G) = T$. Moreover, as the total content of additive in the slurry is given and constant, there is a unique relationship between the additive fraction x and the solid mass fraction in the multi-phase flow, χ_S. Consequently, for a given temperature T, the actual solid fraction χ_S differs from that at equilibrium, $\chi_{S,eq}$, and the difference $(\chi_{S,eq} - \chi_S)$ also measures the distance of the system from equilibrium. Whatever its expression, the distance from equilibrium is the driving force for phase change. The ratio between $(\chi_{S,eq} - \chi_S)$ and $\dot{\chi}_S$ introduces a *kinetics time constant* τ according to:

$$\dot{\chi}_S = \left(\chi_{S,eq}(T) - \chi_S\right) \Big/ \tau \tag{12}$$

When τ is constant, eq. (12) is a kinetics law of the first order. It becomes a general law when τ may depend on the actual state of the slurry, e.g. on microscopic parameters such as the number of crystallites per unit volume or their diameter, quantities that are beyond the scope of this study. Herein, only constant values of τ are considered, but over such a wide range

(from 1 to 1000s) that the detailed mechanisms of kinetics become less significant than the effects of that time constant.

In steady-state, the total derivative $d\chi_S / dy$ of eq. (11) becomes $\dot{\chi}_S / u$, where u is the flow velocity. Resolution of eq. (11) also requires the kinetics law to be expressed in terms of temperature, i.e. with the temperature difference $(T - T_{eq})$ as the driving force for phase-change. At this point, two cases arise.

4.1.1 Slurries IG and TB, without CO_2.

There is no vapor phase flowing with these slurries; one thus has $T_{eq}(x, P_G) \equiv T_{eq}(x)$ and $\chi_S = X$. Once the composition x_0 of the initial water-additive liquid solution is given, there is a unique relationship between the equilibrium temperature and the crystal mass fraction X in the slurry. One point (T, X) describing the system out-of-equilibrium can thus be associated with two points in equilibrium: (T_{eq}, X) and (T, X_{eq}), as shown in Figure 3. The difference $\left(\chi_{S,eq}(T) - \chi_S \right)$ of eq. (12) thus can be translated into a temperature difference $\left(T - T_{eq}(\chi_S) \right)$. The rate of phase-change is then written as $\dot{\chi}_S = \left(T - T_{eq}(\chi_S) \right) \big/ (\beta \tau)$, where β stands for the partial derivative $\left(\partial T_{eq} / \partial \chi_S \right)_m$ at constant total mass in the solid-liquid slurry. The parameter β is derived by combining the equation of state $T_{eq}(x)$ and the conservation of additive between liquid and solid ($\beta < 0$):

$$\beta = \left(dT_{eq} / dx \right) \cdot \left(\partial x / \partial \chi_S \right)_m \tag{13}$$

Along the heat exchangers, the compositions of the liquid phase and the equilibrium temperature change according to the amount of solid crystallized or melted.

14
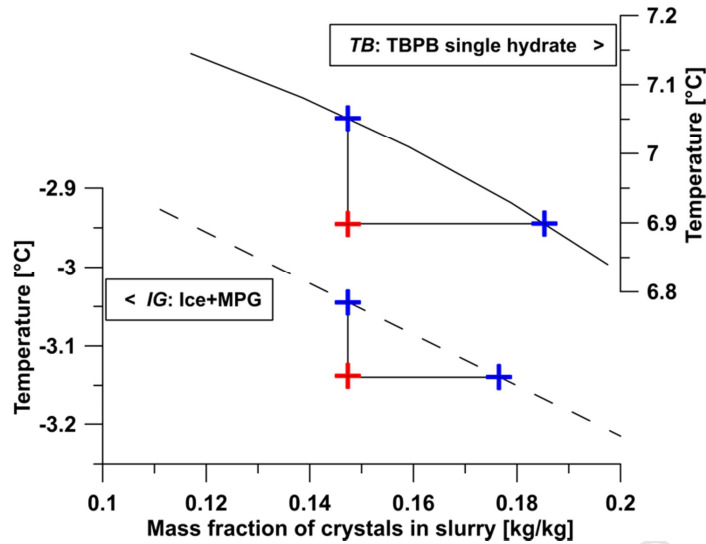
Fig. 3: Description of out-of-equilibrium states for the slurries *IG* and *TB* in the (T, X) axes. The two lines (dashed for *IG*, solid for *TB*) represent equilibrium. One system out-of-equilibrium (+) can be associated with two systems in equilibrium (+): one with the same temperature, one with the same mass fraction of crystals.

4.1.2 Slurries CO and MH, with CO_2.

For these two slurries, the gas pressure P_G is a state variable. For the *CO* system the equilibrium variance is one and the equilibrium temperature depends on the gas pressure alone: $T = T_{eq}(P_G)$. For the *MH* system, the equilibrium variance is two, and the equation of state is $T = T_{eq}(x, P_G)$. Carbon dioxide also plays a role in the kinetics. The phrase *phase change kinetics* is given a strict meaning in this article, i.e. as an intrinsic phenomenon occurring between the solid and liquid phases exclusively. Any transport phenomenon related to phase change, e.g. dissolution of CO_2 into water, transport of CO_2 or of additive in the liquid phase, or heat transfer by conduction/advection, is assumed to be non-limiting, e.g. due to efficient mixing by turbulence. Concentrations and temperature are thus assumed uniform in the slurry, and the rate of phase change $\dot{\chi}_S$ is governed by the kinetics law (12). As phase change equilibrium and distance from equilibrium depend on the interactions between the solid and liquid phases, the governing parameters are temperature, solid mass fraction χ_S,

15

concentration x of TBPB in the liquid phase (when relevant), and concentration of CO_2 dissolved in the liquid phase. The latter concentration is described by the solubility σ of CO_2 in the aqueous phase in equilibrium with CO_2 vapor at pressure P_G defined as:

$$\sigma = \chi_{CD,L} / (\chi_{W,L} + \chi_{CD,L}) = \sigma_{eq}(T_{eq}, P_G) \tag{14}$$

Combining the equation of state $T_{eq}(x, P_G)$ with eq. (14) makes the equilibrium temperature T_{eq} a function of x and σ, the differential of which is $dT_{eq} = (\partial T_{eq}/\partial\sigma)_x \cdot d\sigma + (\partial T_{eq}/\partial x)_\sigma \cdot dx$. Moreover, the amounts of TBPB and carbon dioxide present in the liquid phase are involved in the mass balance invoked by the partial derivative at constant total mass $(\partial T_{eq}/\partial\chi_S)_m = \beta$. Mass conservation for TBPB and CO_2 between solid and liquid leads to the two derivatives $(\partial\sigma/\partial\chi_S)_m$ and $(\partial x/\partial\chi_S)_m$. The expression of β can be obtained directly as:

$$\beta = (\partial T_{eq}/\partial\sigma)_x \cdot (\partial\sigma/\partial\chi_S)_m + (\partial T_{eq}/\partial x)_\sigma \cdot (\partial x/\partial\chi_S)_m$$

These four partial derivatives are detailed in the Appendix.

4.2 Enthalpy balance with kinetics

Combining the kinetics law $\dot{\chi}_S = (T - T_{eq}(\chi_S)) / (\beta\tau)$ with the enthalpy balance (11) leads to:

$$\dot{m} \cdot \left[\overline{c_p} \cdot \frac{dT}{dy} - \Delta H_f \cdot \frac{T - T_{eq}}{\beta\tau u} \right] = U_\bullet \Pi_\bullet \cdot (T_\bullet - T) \tag{15}$$

Each heat exchanger is sub-divided into sections where the mass fraction χ_S changes by a prescribed quantity $\Delta\chi_S$ that is small enough for the various parameters ($\overline{c_p}$, $U\Pi$, β, u) to be

assumed constant as well. The equilibrium temperature T_{eq} governing the phase-change

driving force can be linearized in each section according to: $T_{eq} = T_{eq,in} + \gamma \cdot (\chi_S - \chi_{S,in})$,

where the index *in* refers to the inlet of the section under consideration. In this framework, the

problem [(15) plus kinetics law] has a solution in the form of:

$$\chi_S = \Gamma + \Lambda y + \sum_{1,2} E_k \, e^{-\mu_k y} \tag{16}$$

and $\quad T = T_{eq,in} + \gamma \cdot \left(\Gamma + \Lambda y + \sum_{1,2} E_k \, e^{-\mu_k y} - \chi_{S,in} \right) + (\beta \tau u) \cdot \left(\Lambda - \sum_{1,2} \mu_k E_k \, e^{-\mu_k y} \right) \quad$ (17)

where the six unknown parameters Γ, Λ, E_1, E_2, μ_1 et μ_2 satisfy the equations:

$$\Lambda \dot{m} \cdot \left(\overline{c_p} \gamma - \Delta H_f \right) = U\Pi \cdot \left[T_E - T_{eq,in} - \gamma \cdot (\Gamma - \chi_{S,in}) - \Lambda \cdot (\beta \tau u) \right] \tag{18}$$

$$\gamma \cdot \Lambda = 0 \tag{19}$$

$$\dot{m}\overline{c_p} \cdot (\beta \tau u) \cdot \mu^2 - \mu \cdot \left[\dot{m} \cdot \left(\overline{c_p} \gamma - \Delta H_f \right) + U\Pi \cdot (\beta \tau u) \right] + \gamma \cdot U\Pi = 0 \tag{20}$$

$$\Gamma + \sum_{1,2} E_k = \chi_{S,in} \tag{21}$$

and $\quad\quad\quad\quad \Lambda - \sum_{1,2} \mu_k E_k = \left(T_{in} - T_{eq,in} \right) \big/ (\beta \tau u) \tag{22}$

The temperature T_{in} and the solid mass fraction $\chi_{S,in}$ are prescribed for the first section (inlet

of the heat exchanger), and they are known for any other section as soon as the previous

section has been resolved. The length of each section Δy is adjusted in order to make the solid

mass fraction change by the same $\Delta \chi_S$ in each section. For the *HXU* heat exchanger, the

external temperature T_U is prescribed and the total length L_{HXU} is calculated as the one for

which the values of χ_S and T at the outlet of *HXU* are such that return to equilibrium falls on

17

the prescribed value X_5. The area A_{HXU} is then obtained by: $A_{HXU} = L_{HXU} \cdot \Pi_U$. For *HXE*, the heat exchange area A_{HXE} is prescribed and the total length of *HXE* is thus adapted for equating A_{HXE} / Π_E. The external temperature T_E (refrigerant evaporation) takes the value for which the values of χ_S and T at the outlet of *HXE* are such that return to equilibrium falls on the prescribed value X_1. The data and formulae used for evaluating the heat transfer and friction coefficients are described in [9].

5   Exergy analysis of the effects of kinetics on global performance

Figure 4 shows how the exergy budget changes with the time constant τ, for the two extreme cases *IG* and *MH*, respectively. One piece of information should be noted at this point: the calculated breakthrough time of the slurry flow in either heat exchanger *HXU* and *HXE* (circuit length divided by slurry velocity) is always of the order of one or two minutes. If merely considering time -and the fact that $\exp(-t/\tau)=0.05$ for $t=3\cdot\tau$- one would expect a kinetics time constant of 100s to have a noticeable effect on phase change in those heat exchangers, and thus on global performance. However, calculations show that the total mechanical energy consumed by the process is scarcely changed with τ=100s, and increases by 5% only for $\tau\approx$200s (slurry *MH*) or 500s (slurry *IG*) and even 1000s with the slurry *TB*. Such values of the time constant are much longer than what would be expected from the breakthrough time of the slurry flow in the heat exchangers.

18
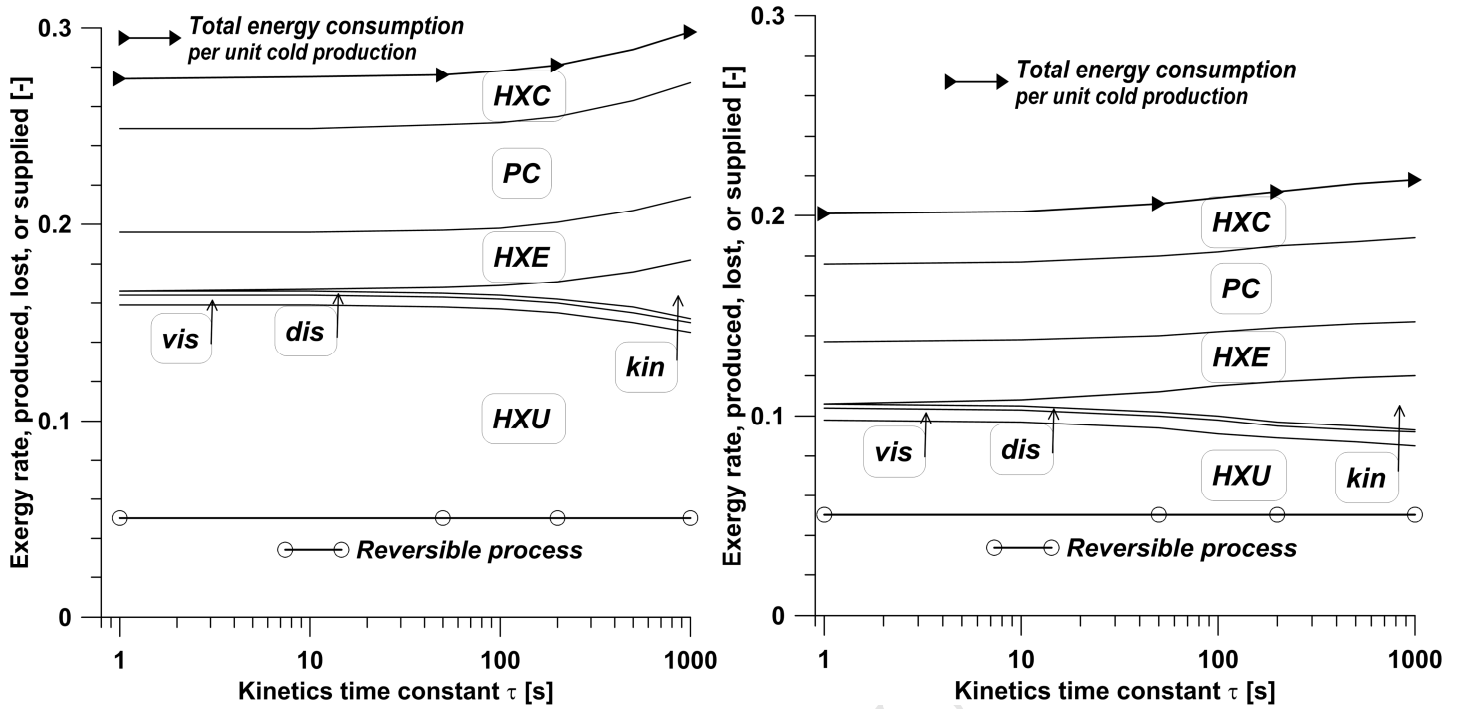
Fig. 4: Effect of the kinetics time constant τ on the non-dimensional performance and exergy analysis for the ice slurry *IG* (left) and for the mixed hydrate slurry *MH* (right). Same legend as in Fig. 2, plus the exergy loss due to phase change kinetics (*kin*).

This counter-intuitive result requires a deeper analysis. Figure 5 displays the profiles of crystal mass fraction χ_S and slurry temperature along the two heat exchangers calculated with τ=1000s for the slurries *IG* and *MH*. The lack of processed (melted or generated) crystals is clearly shown; it is very significant for the slurry *MH*. However, constraint #1 prescribing extraction of the heat flux $\dot{Q}_U = 30kW$ from the end user is always satisfied: the very slow kinetics does not prevent the duty from being fulfilled. Indeed, the temperature shift acting as a working force for phase change (up to 4.8 and 6.3K for *IG* and *MH*, respectively) involves an amount of sensible heat (18.8 and 23.7kJ.kg^{-1}, respectively) that compensates the lack of latent heat (-18.3, and -23.4kJ.kg^{-1}, respectively). In other words, the temperature shift that drives the phase change also reduces the need of phase change for a prescribed transferred heat flux $\dot{Q}_U$. This temperature shift has other consequences, which are specific to each exchanger.

19
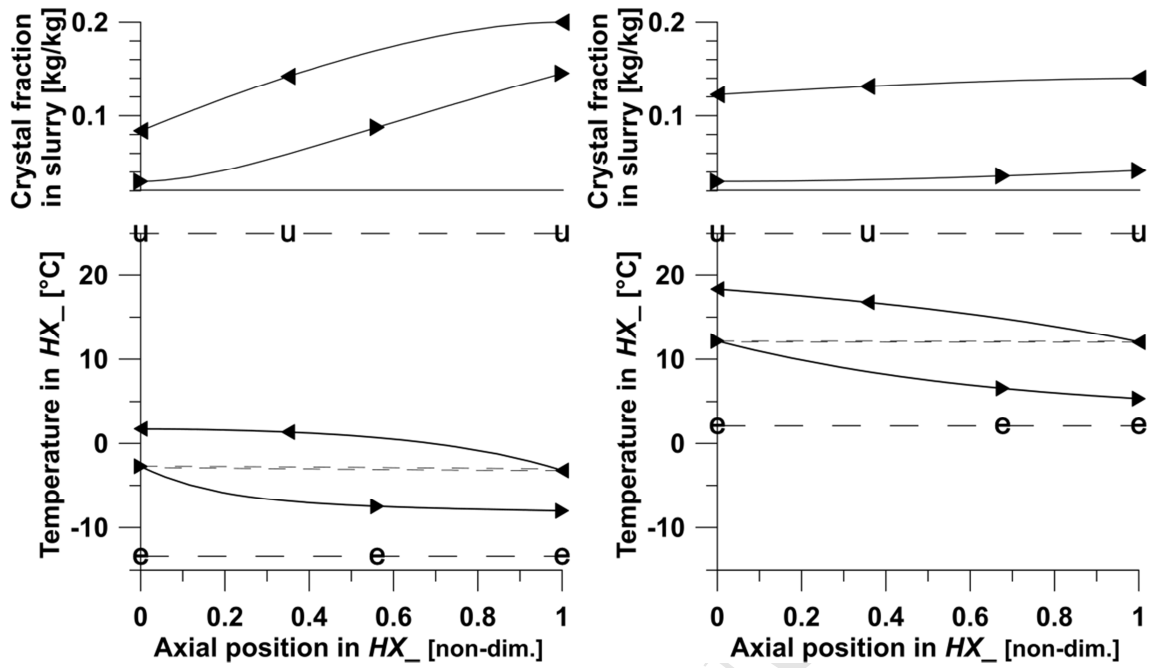
Fig. 5: Profiles in the heat exchangers with kinetics time constant τ=1000s for the two slurries *IG* (left) and *MH* (right): crystal mass fraction (top) and temperatures (bottom), presented with a rightward flow in the evaporator *HXE* (symbols ⏷), and a leftward flow in *HXU* (symbols ▭). The indoor and evaporation temperatures (respectively u and e) are also reported.

5.1 Crystal melting in HXU

As a first consequence, the average temperature difference between indoor air and slurry is reduced. When using the values of entropic mean temperatures, the difference $T_U - T_{34}$ decreases by 3.3K for both slurries, *i.e.* by 12 and 25% for *IG* and *MH* respectively. In order to transfer the same heat flux $\dot{Q}_U$, the heat exchange area A_{HXU} must be extended accordingly, i.e. by 0.7 and 3.4m^2, respectively. It results from that area extension that the corresponding exergy loss Δb_{HXU} drops by 13 and 27% for *IG* and *MH* respectively, as shown in Fig. 4. These ratios are fully in line with the above-mentioned reduction of the temperature difference $T_U - T_{34}$. This development perfectly illustrates the specificity of the present approach where the constraints are explicit and based on an engineering point of view.

If the time constant τ alone were changed (i.e. with the implicit constraint that all the heat exchange areas are kept constant), then the heat flux $\dot{Q}_U$ would also change, and the study would compare equally sized units but with different duties. The same design cannot be optimal for all of them. In the present approach, each unit under consideration is sized according to its own thermophysical characteristics, while fulfilling explicit global constraints that enable a fair comparison.

The changes described above have another consequence: the area of the condenser *HXC* is reduced so that the total area $A_{HXU}+A_{HXC}$ is kept constant (constraint #3). As the area A_{HXC} is much larger than A_{HXU}, its relative reduction is 2 and 13% only, for *IG* and *MH* respectively. This area reduction makes both the condenser temperature T_C and the exergy loss Δb_{HXC} increase, the former by 0.2 and 0.7K, the latter by 3 and 12%, for *IG* and *MH* respectively. As the contribution of *HXC* to the total irreversibility is weak (11 and 17% respectively), the effect on global performance ranges from completely negligible for *IG* to weak for *MH*. It can be seen, however, that the case *MH* with τ=1000s reaches a limit beyond which any further extension of the area A_{HXU} will have a non-negligible impact on Δb_{HXC}. This short development shows how the interaction between components and phenomena may operate and demonstrates the interest of using global approaches to address energy-efficiency challenges.

5.2 Crystal generation in HXE

When the phase change kinetics slows down, crystal generation also occurs with a temperature shift, which is almost symmetrical to that occurring during fusion as shown in Fig. 5. However, the area A_{HXE} is prescribed (constraint #2). Consequently, when the average slurry temperature decreases (T_{51} decreases by 3.5K for both slurries), the evaporation temperature does as well, practically in parallel to each other (-3.9 and -2.3K respectively),

depending on the changes in heat-transfer parameters. The evaporation temperature has a direct influence on the mechanical energy consumed by the primary compressor; in the present framework (prescribed duty and given internal efficiency), the compression power rate should be proportional to $(T_C - T_E)/T_E$. With the values given above, the ratio $(T_C - T_E)/T_E$ increases by 9.0 and 8.8%, for *IG* and *MH* respectively. These figures fully explain the 8.8% increase in consumed energy for both slurries. As when comparing various slurries, the changes in evaporation temperature almost entirely account for the observed changes in energy efficiency.

5.3   A question of temperature with various couplings

Figure 6 presents the changes in the entropic mean temperatures T_{34} and T_{51} for both slurries when τ changes from 1 to 1000s, and to relate them to the other important temperatures with respect to energy efficiency. As expected, the respective shapes of these four curves reproduce the changes in exergy losses due to kinetics displayed in Fig. 4. One of these graphs highlights how the *HXU* heat exchanger is affected by the temperature shift due to melting kinetics: for the secondary refrigeration process to maintain its duty, the size of this exchanger must be adapted to the actual value of $T_U - T_{34}$, the relative variation of which may be significant. The other graph highlights the temperature difference that governs the energy consumption of the process: $T_C - T_E$. This temperature difference is much greater than the former one, its relative variation thus remains weak. This is why phase change kinetics has a quite limited effect on energy efficiency. It is, however, important to stress that this conclusion holds true on the condition that the design of the heat exchangers accounts for the thermal effects of kinetics.
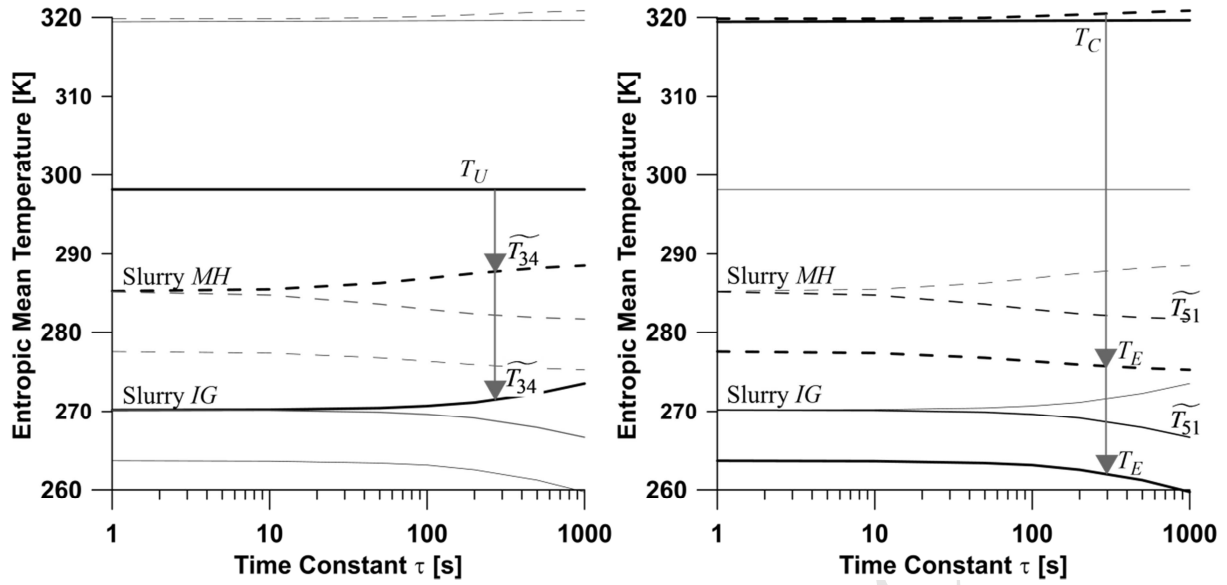
Fig. 6: Entropic mean temperatures T_{34} and T_{51} as functions of the kinetics time constant, and interpretation with respect to energy efficiency. Left side: Transfers in HXU are ruled by the temperature difference $T_U - T_{34}$, represented by the grey vertical arrows. Right side: total energy consumption is mainly governed by the temperature difference $T_C - T_E$ (grey vertical arrows), with the latter temperature following the variations of T_{51}.

6   Accuracy assessment

Some data used in the present calculations are uncertain, particularly the viscosity and the heat transfer coefficients. The dependence of the present results on those quantities, as well as on the latent heat of fusion (often invoked as an important parameter for energy efficiency) and the internal efficiency of the primary cooling cycle, has been investigated. The latent heat and the heat transfer coefficient on the slurry side of heat-exchange were both changed by the factors 0.9 and 1.1, the apparent viscosity of the slurry was changed by the factors 2/3 and 1.5. Lastly, a reduction of the primary cycle efficiency η_{PCU} by 6% was also tested. The data, presented in Fig. 7, first show that the resulting dispersion on the total energy consumption cannot change the ranking between the four slurries. The qualitative result of this study still holds: the melting temperature remains the most influential parameter with respect to energy efficiency. In a second time, among the quantities tested in this section, the efficiency η_{PCU}

appears to be the most influential on global energy efficiency. Indeed, most of the energy consumption of the process is that of the primary compressor. Reducing the efficiency of the primary cycle directly increases the latter energy consumption by the same proportion, whatever the slurry. The ranking between slurries remains the same. Among the slurry properties, the heat transfer properties are the next influential parameters. Indeed, they have a direct effect on the evaporation temperature, and therefore on the primary cycle efficiency. The other properties, latent heat and viscosity, are the least influential ones.
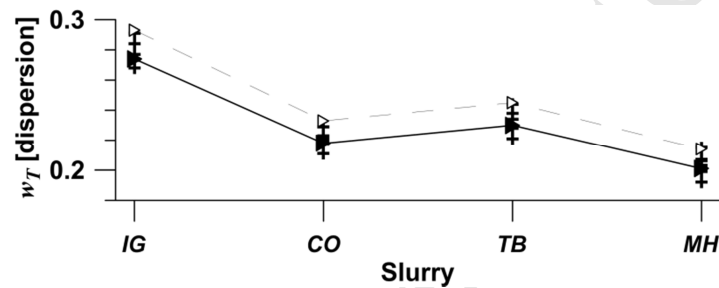

Fig. 7: Dispersion of the calculated values of w_T. Closed triangles ► with solid line: values of Fig. 2. Crosses +: dispersion obtained with changes in latent heat, viscosity, or heat transfer coefficients. Open triangles ▷ with dashed line: reduction of η_{PCU}.

7   Conclusion

All the information shown by the present analysis can be summarized as follows. The energy efficiency of secondary refrigeration with prescribed duty depends primarily on the evaporation temperature T_E, or more precisely on the ratio $(T_C - T_E)/T_E$, where T_C is the condensation temperature. These two temperatures are internal temperatures and are highly dependent on other design parameters. The first of these is the melting temperature of the selected slurry. This temperature is important because it creates a link between the irreversibility due to heat transfer from user to slurry and the evaporation temperature. This link explains how a reduction in that exergy loss directly induces a decrease in the power consumed by the primary compressor.

Introducing kinetics into the analysis splits the notion of phase change temperature, which is unique when in equilibrium, into two different effective temperatures, one for crystal fusion and the other for crystal generation. The former temperature helps sensible heat to compensate for the lack of latent heat caused by kinetics. The latter temperature directly influences the evaporation temperature T_E, and indirectly affects the energy efficiency of the whole process via the ratio $(T_C - T_E)/T_E$. The irreversibility related to kinetics can be interpreted clearly when using the notion of entropic mean temperature.

Finally, the analysis demonstrates that, from the viewpoint of energy efficiency, temperature is more important than time when considering the effects of phase change kinetics.

Acknowledgement

Appendix: Partial derivatives in the expression of β

The total derivatives of the general equation of state $T_{eq}(x, P_G)$ and of the solubility $\sigma_{eq}(T_{eq}, P_G)$ of CO_2 in water are: $\quad dT_{eq} = \left(\partial T_{eq}/\partial P_G\right)_x \cdot dP_G + \left(\partial T_{eq}/\partial x\right)_{P_G} \cdot dx \quad$ and

$d\sigma = \left(\partial \sigma_{eq}/\partial T_{eq}\right)_{P_G} \cdot dT_{eq} + \left(\partial \sigma_{eq}/\partial P_G\right)_{T_{eq}} \cdot dP_G$. Combining them leads to:

$$\left(\frac{\partial T_{eq}}{\partial \sigma}\right)_x = \frac{\left(\partial T_{eq}/\partial P_G\right)_x \cdot dPds}{1 - \left(\partial T_{eq}/\partial P_G\right)_x \cdot dPdT} \ , \ \left(\frac{\partial T_{eq}}{\partial x}\right)_\sigma = \frac{\left(\partial T_{eq}/\partial x\right)_{P_G}}{1 - \left(\partial T_{eq}/\partial P_G\right)_x \cdot dPdT} \tag{A.1}$$

where *dPds* and *dPdT* are given by:

$$dPds = \frac{1}{\left(\partial\sigma_{eq}/\partial P_G\right)_{T_{eq}}} \quad , \quad dPdT = \frac{-\left(\partial\sigma_{eq}/\partial T_{eq}\right)_{P_G}}{\left(\partial\sigma_{eq}/\partial P_G\right)_{T_{eq}}}.$$

The expressions of σ, eq. (14), and of x, $x = \chi_{A,L}/\left(\chi_{A,L} + \chi_{W,L}\right)$, lead to the following relations:

$$\frac{\chi_{CD,L}}{\chi_L} = \frac{\sigma\cdot(1-x)}{(1-x\cdot\sigma)} \ , \ \frac{\chi_{A,L}}{\chi_L} = \frac{x\cdot(1-\sigma)}{(1-x\cdot\sigma)}, \ \text{and} \ \frac{\chi_{W,L}}{\chi_L} = \frac{(1-x)\cdot(1-\sigma)}{(1-x\cdot\sigma)} \quad (A.2)$$

Mass conservation in the solid-liquid slurry is written: $\mathrm{d}\chi_{\bullet,L} + Y_\bullet\cdot\mathrm{d}\chi_S = 0$, where $\bullet$ stands for CD, A, or W. Combining the latter relation with the first two equations of (A.2) leads to the following set of two equations:

$$
\begin{aligned}
(1-x)\cdot\mathrm{d}\sigma - \sigma\cdot(1-\sigma)\cdot\mathrm{d}x &= \left[Y_{CD}\cdot(1-x\cdot\sigma)^2 + \sigma\cdot(1-x)\cdot(1-x\cdot\sigma)\right]\cdot\mathrm{d}\chi_S \\
-x\cdot(1-x)\cdot\mathrm{d}\sigma + (1-\sigma)\cdot\mathrm{d}x &= \left[Y_A\cdot(1-x\cdot\sigma)^2 + x\cdot(1-\sigma)\cdot(1-x\cdot\sigma)\right]\cdot\mathrm{d}\chi_S
\end{aligned}
\quad (A.3)
$$

A straightforward resolution gives the partial derivatives:

$$
\begin{aligned}
\left(\partial x/\partial\chi_S\right)_m &= (Y_A + x + x\cdot Y_{CD})\cdot(1-x\cdot\sigma) \ / \ (1-\sigma) \\
\left(\partial\sigma/\partial\chi_S\right)_m &= (Y_{CD} + \sigma + \sigma\cdot Y_A)\cdot(1-x\cdot\sigma) \ / \ (1-x)
\end{aligned}
\quad (A.4)
$$

Bibliography

[1] Bellas I, Tassou SA. Present and future applications of ice slurries. Int J Refrig. 2005;28(1):115-21.

[2] Cowan D, Gartshore J, Chaer I, Francis C, Maidment G. REAL Zero – Reducing refrigerant emissions & leakage - feedback from the IOR Project Proc Inst R 2009-10: IOR The Institute Of Refrigeration; 2010. p. 16.

[3] Sloan ED, Koh CA. Clathrate Hydrates of Natural Gases Third Edition Preface. 3rd ed. Boca Raton, FL: CRC Press-Taylor & Francis Group, 2008.

[4] Mayoufi N, Dalmazzone D, Delahaye A, Clain P, Fournaison L, Fuerst W. Experimental Data on Phase Behavior of Simple Tetrabutylphosphonium Bromide (TBPB) and Mixed CO2 + TBPB Semiclathrate Hydrates. Journal of Chemical and Engineering Data. 2011;56(6):2987-93.

[5] Lin W, Dalmazzone D, Fuerst W, Delahaye A, Fournaison L, Clain P. Thermodynamic properties of semiclathrate hydrates formed from the TBAB plus TBPB plus water and CO2 + TBAB + TBPB plus water systems. Fluid Phase Equilib. 2014;372:63-8.

[6] Liu WG, Wang SR, Yang MJ, Song YC, Wang SL, Zhao JF. Investigation of the induction time for THF hydrate formation in porous media. J Nat Gas Sci Eng. 2015;24:357-64.

[7] Aman ZM, Akhfash M, Johns ML, May EF. Methane Hydrate Bed Formation in a Visual Autoclave: Cold Restart and Reynolds Number Dependence. Journal of Chemical and Engineering Data. 2015;60(2):409-17.

[8] Mahmoudi B, Naeiji P, Varaminian F. Study of tetra-n-butylammonium bromide and tetrahydrofuran hydrate formation kinetics as a cold storage material for air conditioning system. J Mol Liq. 2016;214:96-100.

[9] Pons M, Hoang H-M, Dufour T, Delahaye A, Fournaison L. Energy analysis of two-phase secondary refrigeration in steady-state operation, Part 1: global optimization and leading parameter. Energy. 2018;submitted.

[10] Pons M. Analysis of the adsorption cycles with thermal regeneration based on the entropic mean temperatures. Applied Thermal Engineering. 1997;17(7):615-27.

[11] Dufour T, Hoang HM, Oignet J, Osswald V, Clain P, Fournaison L, et al. Impact of pressure on the dynamic behavior of CO2 hydrate slurry in a stirred tank reactor applied to cold thermal energy storage. Applied Energy. 2017;204:641-52.

[12] Uddin M, Coombe D. Kinetics of CH4 and CO2 Hydrate Dissociation and Gas Bubble Evolution via MD Simulation. J Phys Chem A. 2014;118(11):1971-88.

[13] Yang D, Le LA, Martinez RJ, Currier RP, Spencer DF. Kinetics of CO2 hydrate formation in a continuous flow reactor. Chemical Engineering Journal. 2011;172(1):144-57.

[14] Jerbi S, Delahaye A, Fournaison L, Clain P, Haberschill P, Int Inst R. CO2 hydrate formation kinetics and modelling of the available enthalpy of CO2 hydrate slurry in tank reactor. 23rd IIR International Congress of Refrigeration2011. p. 2191-8.

Highlights

- Entropic mean temperatures of non-isothermal heat exchangers lead to exergy

- The exergy budget of secondary refrigeration process is fully established

- The exergy loss between user and slurry influences the total energy consumption

- The size of heat exchangers must account for kinetic effects

- Then, energy efficiency is weakly affected by kinetics